HVAC&R Research
Publication details, including instructions for authors and subscription information:
http://www.tandfonline.com/loi/uhvc20

Efficient Horizontal Ground Heat Exchanger Simulation with Zone Heat Balance Integration

Edwin S. Lee [a] , Daniel E. Fisher PhD PE [b] & Jeffrey D. Spitler PhD PE [c]

[a] Student Member ASHRAE, Research Assistant, Oklahoma State University

[b] Fellow ASHRAE, E. Fisher Professor, Oklahoma State University

[c] Fellow ASHRAE, Regents Professor and C. M. Leonard Professor, Oklahoma State University

Accepted author version posted online: 21 Feb 2013.

To cite this article: Edwin S. Lee , Daniel E. Fisher PhD PE & Jeffrey D. Spitler PhD PE (2013): Efficient Horizontal Ground Heat Exchanger Simulation with Zone Heat Balance Integration, HVAC&R Research, DOI:10.1080/10789669.2013.774887

To link to this article: http://dx.doi.org/10.1080/10789669.2013.774887

Efficient Horizontal Ground Heat Exchanger Simulation with Zone Heat Balance Integration

Corresponding Author:

Edwin S. Lee

Student Member ASHRAE

Research Assistant

Oklahoma State University

e.lee@okstate.edu

Co-authors:

Dr. Daniel E. Fisher, PhD, PE

Fellow ASHRAE

E. Fisher Professor

Oklahoma State University

dfisher@okstate.edu

Dr. Jeffrey D. Spitler, PhD, PE

Fellow ASHRAE

Regents Professor and C. M. Leonard Professor

Oklahoma State University

Spitler@okstate.edu

Author details for first page footer:

Edwin S. Lee, Student Member ASHRAE, is Research Assistant. **Daniel E. Fisher, PhD, PE**, Fellow ASHRAE, is E. Fisher Professor. **Jeffrey D. Spitler, PhD, PE**, Fellow ASHRAE, is Regents Professor and C. M. Leonard Professor.

For horizontal heat exchangers buried near a building slab or basement, interaction between the heat exchanger and the zone can be significant. Thermal interference effects can also be significant for heat exchangers with multiple pipes in close proximity. Previous simulation methodologies have not modeled these phenomena in a general manner and have lacked integration with other simulation domains including zone heat balance calculations and fluid loop solvers.

A numerical model for horizontal ground heat exchanger applications is presented, featuring a computationally efficient mesh and flexible heat exchanger tube placement. The model integrates the ground with zone heat balance and hydronic system simulations through boundary conditions within a whole building energy simulation program. Thermal interference between pipes is captured including circuiting effects of the fluid flow direction in individual pipes.

Validation is performed using experimental data from a foundation heat exchanger research facility. Undisturbed ground temperature data is used to estimate ground and boundary

properties. The model predicts heat pump entering fluid temperature with mean error of 1.3°C (2.3°F) and basement wall heat flux with mean error of 1.1 W/m^2 (0.35 btu/hr-ft^2). This accuracy is achieved with a coarse grid, ensuring a small computational burden suitable for whole building energy simulation.

Background

Stricter energy standards are increasing the requirements of building modeling. Guidelines have been provided by Stocki, Curcija, & Bhandari (2007) relating to proper model parameters and assumptions, though no details were provided for handling ground heat transfer effects. Thomas & Rees (2009) showed that the earth heat transfer through building floors can be significant, while other works (Adjali, Davies, & Rees 2004; Andolsun, Culp, & Haberl 2010) have shown that there is much uncertainty in ground heat transfer prediction based upon modeling approach and inputs. Ihm & Krarti (2004) developed a detailed foundation heat transfer model and implemented it in EnergyPlus (Crawley, et al. 2001), improving the heat transfer modeling capabilities for ground-coupled zones.

Using the ground as a heat sink or heat source has been studied for decades, including simulation work such as Claesson & Dunand (1983). Smaller energy footprints of highly efficient buildings have opened the door for new heat exchanger configurations, including placement in the near-field of a building foundation or basement (Cullin, et al. 2012; Xing, et al. 2011; Den & Nielsen 1998). These foundation heat exchangers have been modeled by Xing, et al. (2011). The current work builds on this with additional simulation capabilities:

- Direct coupling to a zone heat balance within a whole building energy simulation environment
- Improved flexibility for pipe placement within the calculation domain
- Capturing enhanced effects including axial temperature distributions, circuiting effects with multiple pipes by relating the outlets of pipe segments to the inlets of downstream segments, and the effects of individual segments' fluid flowing in different directions
- Improved computational efficiency using an intelligent mesh scheme

Foundation heat exchangers specifically have also been modeled by Rees, et al. (2012) using a dynamic thermal network approach. A step response is calculated on a detailed three dimensional finite volume domain and used in the dynamic thermal network system of equations to calculate the system response during a simulation. The dynamic thermal network approach allows ultimate flexibility, provided the response factors can be generated, and while the resulting response factor model is computationally efficient, creating the response factors requires a detailed, computationally burdensome technique. In the context of whole building energy simulation, computational burden is a focus, and so the current model balances flexibility with computational effort. The dynamic thermal network assumes a uniform fluid boundary condition for the entire fluid surface, while the current model allows flexible circuiting such that fluid may enter the domain in pipe circuits at widely different conditions, and still be captured in the overall domain response.

These foundation heat exchangers provide a possible alternative to traditional ground heat exchangers which may be limited due to cost or space constraints. The limitation of such heat exchangers is due to the close proximity to the building. This has the potential for significant

feedback between the ground heat exchanger and the zone. This model is designed to handle these heat exchanger applications by improving not only the ground heat transfer modeling capabilities, but also the integration between building simulation domains.

The model is not only applicable to foundation heat exchangers, but also horizontal heat exchangers and district heating or cooling systems. The grid generation techniques used make this model suitable for simulation of long piping systems, as the computational mesh is refined in areas where the thermal interaction is highest, and the model is proven to provide accuracy with a highly coarse grid.

In addition, the model can be applied to niche configurations, including modeling the supply water pipe from a utility junction to a building, modeling the horizontal legs between vertical boreholes in a ground heat exchanger field, and multiple pipe configurations with heating, cooling, or neutral pipes running in proximity. The model fully accounts for the effects of circuiting and flow direction and is suitable for implementation in a whole building energy analysis program.

Preliminary Modeling Discussion

Existing horizontal ground heat exchanger models have three shortcomings when applied to novel configurations in whole building energy simulation. The first is the lack of generality. Approaches using a line source allow generalized pipe placement (multiple pipes with superposition), but are limited in integration capabilities. Building simulation fluid loop solvers using a flow-wise component-by-component simulation order are designed for component models that input entering fluid conditions and return fluid exiting conditions. The line source model is driven instead by the line source intensity, or the heat rejection rate of the source.

Several studies (Ingersoll & Plass 1948; Den & Nielsen 1998; Chengju, Changsheng, & Kai 2012) utilized line source theory to simulate buried pipes and heat exchangers. Other studies (Ngo & Lai 2005; Sadegh, Jiji, & Weinbaum 1987) used a simplified representation of the fluid as a boundary condition to the ground domain.

The second shortcoming is the lack of coupling to component model based fluid loop simulation engines. A fluid loop simulation engine, in the current context, refers to system simulation models that rely on linking independent components together to result in an overall system response. This relies on the ability of component models to capture a variation of fluid state (transit effect) through the model, from an inlet to an outlet. Numerous studies on buried pipes or heat exchangers (Bau & Sadhai 1982; Bronfenbrener & Korin 1999; Chung, Jung, & Rangel 1999; Esen, Inalli, & Esen 2007; Said, et al. 2009) modeled the fluid without capturing the axial fluid variation, limiting the possibility of performing whole system evaluation. Other simulation models capture fluid variation from inlet to outlet, making them suitable for implementation in a fluid loop simulation engine. Yavuzturk & Spitler (1999) described a vertical ground heat exchanger model that relies on response factors to calculate the fluid response through the heat exchanger, by relating the heat transfer to the mean borehole temperature. The ability to track fluid conditions from an inlet state to an outlet state allowed this model to become the basis for the vertical ground heat exchanger model in EnergyPlus (Fisher, et al. 2006). The model presented in the current work is formulated differently from Yavuzturk & Spitler (1999), yet follows the inlet state to outlet state procedure to fit with the fluid loop simulation model. Tobias (1973) used an approximation of the fluid response in the system to allow fluid transit to be captured in simplified models. Mei (1988) and Piechowski

(1999) utilized specialized coordinate systems to capture the fluid transit with either one or two pipes in the domain. The dual coordinate system approach for embedding pipes in the domain by Piechowski (1999) is a suitable starting point for developing a generalized horizontal ground heat exchanger model, because the grid is refined in the near pipe region, without the need for a complicated or highly dense coordinate system.

The third shortcoming in existing models is the lack of integration between the ground and nearby building zones. In general, zones refer to a physical building space, such as a basement. However, in simulation the term zone may be used as a concept for an artificially dividng portion of a building space. In either case, for whole building energy simulation programs, ground heat transfer models must be integrated with the zone heat balance calculations to account for dynamic thermal feedback. Binks (2011) noted the importance of accurate ground temperature prediction for building simulation, though zone heat balance simulation models generally use a simplified representation of the ground, utilizing a direct boundary condition on the bottom of the ground-coupled floor surface. Cullin, et al. (2012) utilized an iterative approach to couple separate zone and ground heat exchanger models when simulating foundation heat exchangers.

This development path resulted from the idea that thermal ground interaction was secondary to other heat transmission in the zone (Claesson & Hagentoft 1991). The interactions between the zone and a ground heat exchanger are secondary in traditional heat exchanger configurations, as there is sufficient distance between the two to decouple them. For low energy applications where these heat flows are more dominant, this assumption can break down.

Coupling the ground, zone, and fluid loop simulation domains is a major contribution of the current model. Simulation mechanics and assumptions vary between simulation programs,

however it is common for the zone heat balance to be a quasi-steady-state solution. Pumping and piping simulation is often similar, with steady state mechanics utilized over a single step in time. Coupling these quasi-steady simulation mechanics to a transient ground simulation model requires special treatment of the various domain hooks. This is further complicated if the simulation domains operate at independent time step levels, such as with the whole building energy simulation tool EnergyPlus (Crawley, et al. 2001). Coupling the different simulation mechanics and independent time integration steps is addressed by the current model which improves the feedback between simulation systems and improving accuracy of the whole building energy simulation environment.

Methodology

The physics of the ground heat exchanger model consists of thermal interaction between a fluid being transported through the domain, the transient ground mass, and the various boundary conditions including the ground surface, zone heat balance, and far-field. The physical domain can contain multiple pipes located near a basement zone, possibly in the excavation area of the ground. By simplifying the geometry into a Cartesian simulation domain and assuming a far-field boundary distance, the corresponding simulation domain is shown in Figure 1. In this figure, the domain cross section contains a basement region, and as an example, there are five tubes placed in the domain. The domain consists of a series of these two-dimensional cross sections extruded uniformly in the axial pipe direction. Thus all pipes and any other objects in the domain are parallel with uniform geometry throughout the axial length. This assumes that any zone interaction exists over the entire length of the domain. When basement walls only exist for a portion of the domain length, multiple domains are implemented, of which some will

include basement interaction and some will not. Based upon the required detail, careful circuiting of the fluid between the domains can be implemented to ensure the fluid path is exactly as in the real system. For the case of foundation heat exchangers, the tubes may wrap around multiple corners of the basement in reality. The model assumptions do not allow this to be applied directly. Instead, the physical domain must be simplified with an effective overall length to capture the corner effects.

Simulation Domain

The simulation domain consists of the ground, plus the integration with the zone and piping systems, along with other boundary conditions. Groundwater movement is not included, but the effects of stagnant moisture content in the soil, including freezing, are simulated. Moisture transport effects are excluded because parameters required for groundwater flow models are only known under specialized conditions. Raymond, et al. (2011) demonstrated (through validation of a numerical model using data from an experimental test site (Austin, Yavuzturk, & Spitler 2000)) that for a significant range of groundwater flow conditions, the effects on a thermal response test are negligible. It is assumed that the inclusion of stationary moisture content can provide sufficient accuracy. Static water content is included using weighted average thermal properties. The freezing is simulated using an effective specific heat over a small temperature range near the freezing point. The total energy within this range is equivalent to the latent heat of melting. This method is described by Lamberg, Lehtiniemi, & Henell (2004).

In general, the ground is governed by a transient energy balance:

$$\frac{\partial T}{\partial t} = \alpha \nabla^2 T \tag{1}$$

This equation is applied to a mesh created in the domain. The coordinate system is Cartesian, suitable for the rectangular domain (Figure 1). Since the domain will contain objects besides just the ground, the mesh is created using a partition approach. Vertical and horizontal partitions are aligned in the domain at the location of each pipe or domain object. A single pipe in the domain, along with the basement surfaces, results in two partitions in each of the x and y directions, as shown in Figure 2a. The partition is a finite size, large enough to contain the pipe or basement surface. Vertical partitions become a single cell wide, and horizontal partitions become a single cell tall as part of the overall mesh.

The regions between the domain partitions are then meshed, as shown in Figure 2b. The mesh may be uniform throughout the region or utilize a symmetric geometric series expansion to define the cell distribution. A uniform mesh distributes the cells evenly. The geometric distribution is calculated based on the number of cells and the expansion coefficient ζ. The geometric distribution is symmetric, thus one side of the region is meshed, then mirrored to the other half. The width of each cell is calculated as:

$$\Delta x_1 = \frac{\Delta x_{region}}{2}\left[\sum_{j=0}^{N_{cells}/2} \zeta^j\right]^{-1} \tag{2}$$

$$\Delta x_i = \Delta x_1 \zeta^i \tag{3}$$

Once complete, the domain may be meshed as in Figure 2b. The number of cells is the same in each mesh region between objects. As partitions get closer, the grid then becomes refined,

which is beneficial as these areas would be expected to have the highest temperature gradients. This refinement is enhanced if the geometric mesh distribution is utilized. The domain is then extruded in the pipe axial direction to provide three dimensional cells.

Coupling: Pipe & Ground

The fluid passes through the three-dimensional domain inside each pipe segment. The flow direction is defined per segment, and the same flow can pass through multiple pipes. This allows a single circuit to have multiple passes within the domain, capturing the effects of flow direction. Multiple circuits can then be placed in the same domain to allow multiple fluid inlets and outlets. The transfer from one segment to another is idealized, the effects of a u-bend at the end of the domain are not simulated. Instead, the fluid information is immediately transferred from one outlet to the next segment inlet.

Figure 3 shows different approaches to simulate the pipe within the Cartesian grid. Utilizing a single temperature for the entire cell, which is an average of the contents in the cell, is shown in Figure 3a. With this method, it is difficult to capture the fluid-soil interaction, as the effects are lumped.

An additional level of detail is shown in Figure 3b, in which the fluid and pipe are explicitly modeled. This is a suitable approach, however, the mesh near the pipe is as coarse as the surrounding Cartesian system. Since this area contains the highest temperature gradients, this region warrants additional refinement.

Utilizing a radial coordinate system embedded within a Cartesian cell was proposed by Piechowski (1996). Figure 3c shows a full radial coordinate system placed within the Cartesian cell. Note that this results in an interface cell which exists at the four corners of the Cartesian

cell boundaries. The surrounding Cartesian system interacts with this interface instead of directly with the embedded pipe cell. The radial system is then utilized to simulate the near-pipe region, and inherently provides a refined mesh in this region.

The fluid in each discretized segment is modeled as a lumped element, limiting the ability to capture angular variation of temperature and heat transfer. To improve computational efficiency, the radial soil cell distribution follows this assumption and includes only one-dimensional radial heat transfer. The calculations are then reduced to an axisymmetric radial system as shown in Figure 3d. All four Cartesian neighbors interact with the interface cell, along with the single radial direction. The current model builds upon the original dual coordinate system approach by Piechowski (1996) with fully generalized pipe placement in the domain.

The thermal interchange between the coordinate systems is governed by the following energy balance:

$$\rho V C_p \frac{\partial T}{\partial t} = \sum \dot{q}_{in,Cartesian} + \dot{q}_{in,radial} \tag{4}$$

For the Cartesian heat transfer calculations, the thermal distance is the distance from the centroid of the neighbor Cartesian cell to the corresponding interface thermal node:

$$R_{Cartesian \rightarrow interface} = \frac{\Delta y_i}{2k_{i,j}\Delta x} \tag{5}$$

For the radial system a standard radial resistance is applied:

$$R_{radial \rightarrow interface} = \frac{ln\left(r_o / r_c\right)}{2\pi k} \tag{6}$$

From the interface inward radially to the pipe wall, the heat transfer is modeled using a transient radial formulation. At the pipe wall to fluid interface, the approach requires special treatment.

Coupling: Pipe & Fluid

Figure 4 shows a number of features related to the fluid cell geometry. The fluid cell is a cylindrical finite volume cell with a representative temperature located at the center of the flow. The fluid inlet is a well-formed boundary condition of temperature and mass flow rate. The pipe wall is a radial finite volume cell with a representative temperature located for thermal network calculations at the radial centroid (see Figure 4). The fluid and pipe cells are coupled via the heat convection at the pipe inner surface. During a given iteration, the pipe wall has a single, uniform temperature. By assuming the entering fluid mixes with the fluid currently existing in the cell, the governing equation is the following energy balance:

$$mC_p \frac{dT_f}{dt} = \dot{m}C_p \left(T_{in} - T_f\right) + UA\left(T_{pipe} - T_f\right) \quad (7)$$

The finite difference formulation of this lumped mass equation for each segment results in the accuracy varying with the axial length of each pipe segment. For smaller segments, the finite difference formulation approaches the governing differential equation behavior. The actual phenomena occurring within the pipe at a given point in the system includes mechanical mixing, thermal diffusion, boundary heat transfer, entry-length effects and varying pipe geometry and piping connections. Assuming the flow is generally turbulent, this equation which assumes mixing provides the accuracy required for whole building simulation applications.

The surface conductance U is calculated as the series radial resistance from the fluid to the pipe wall radial centroid, thus including convection and conduction. For turbulent flow, the convection coefficient is calculated based on current fluid conditions using a well-accepted form of the Nusselt correlation by (Dittus & Boelter 1930):

$$Nu_D = 0.023 Re_D^{0.8} Pr^n \quad \left[Re_D \square 10000 \right] \tag{8}$$

The exponent n is set to 0.4 when the fluid is being heated and 0.3 when the fluid is being cooled. This equation is an explicit expression for Nusselt number that assumes a uniform set of properties over the fluid. In heat exchanger applications of this model, the temperature variation is low enough to allow the use of such an equation. During simulations presented in this paper, the Reynolds number periodically dropped out of the stated Reynolds number range, however the majority was well within the valid range, and the lower bound on Reynolds is an approximate lower bound, not a well-defined limit.

Although laminar flow conditions are not expected in heat exchanger applications, this model uses a constant value of Nusselt number as shown in Equation 9 for low Reynolds Number conditions. The constant value is an analytic solution assuming fully developed, steady, one-dimensional flow in a circular tube with a constant surface temperature, the applications for this model do not warrant a more detailed approach:

$$Nu_D = 3.66 \quad \left[Re_D < 2300 \right] \tag{9}$$

Under zero-flow conditions, a prescribed convection coefficient simulates the free convection heat transfer in the pipe. The fluid cells are simulated flow-wise beginning from the circuit inlet cell and downstream to the circuit outlet cell. Circuit inlet conditions are well-

formed from other components in the fluid loop simulation system. This flow-wise simulation captures directional flow circuiting effects, allowing detailed studies of varying flow direction to be performed.

Integration: Fluid Loop Simulation

The fluid heat transfer within the pipe is governed by the equations in the previous section. The fluid circuit inlets and outlets of this model are then connected to a fluid loop simulation within the whole building energy analysis program. At each iteration, the fluid circuit inlet provides mass flow rate and energy boundary conditions. The fluid is simulated through the circuit until at the fluid outlet, which is governed by the continuity and the energy balance on the outlet cell of the circuit (Equation 7). The loop simulation is quasi-steady state, operating at a time step which varies to ensure system convergence is attained. The ground domain is fully dynamic, thus the coupling between the two domains acts as an interface between time stepping paradigms. The pipe and soil cells near the pipe (within the radial coordinate system) iterate concurrently with the fluid loop, responding to the rapid changes in the fluid conditions. The remaining cells are updated on a zone-level time step, which will be equal to or larger than the fluid loop time step. This dual time step approach focuses computational burden, allowing the broad ground domain to update less frequently while still capturing the rapid transients of the near-pipe region. The interface cell between coordinate systems then act not only as a grid interface, but also a time step interface. Typical time step values are fifteen minutes for the zone-level and as low as 1 minute for the fluid loop simulation. At these levels, the near-pipe cells would be updated over fifteen time steps over which time the remaining ground domain will not be updated. This corresponds well with the expected response times of each region.

Integration: Zone Heat Balance

Integrating the zone heat balance with the ground simulation, and therefore with the fluid in the heat exchanger captures the thermal feedback between the two systems. The zone heat balance is governed by Equation 10, which is a transient energy balance of thermal phenomena in a zone. The first term on the right hand side is the sum of internal gains in the space (people, equipment, lights). The second term represents the infiltration gain on the space. The third term represents the convective heat transfer from each surface in the space to the air. The final term represents the energy provided by system conditioning equipment:

$$m_a C_{p,a} \frac{\partial T_a}{\partial t} = \sum_{i=1}^{N} \dot{q}_{int,i} + \dot{q}_{inf} + \sum_{i=1}^{N_{surf}} \dot{q}_{conv} + \dot{q}_{sys} \qquad (10)$$

The zone air is then connected thermally with the zone surfaces via the convective heat transfer rate, governed by Newton's law of cooling:

$$\dot{q}_{conv} = hA\left(T_{surface} - T_a\right) \qquad (11)$$

The convection coefficient, h, is a function of several variables, depending on the model used for the zone air conditioning. Generally it will be a function of diffuser type and location, surface orientation and overall zone air flow rate.

The heat transfer through the building surface (typically the basement wall or floor) is transient conduction, which is typically modeled using a conduction transfer function method or a finite difference algorithm. Conduction transfer functions are used widely in whole building energy simulation due to the lightweight computational burden. Response factors are generated one time for each construction, and these are then used in a time series calculation to determine the response of the surface. For calculating the heat flux on the inside of a building surface,

using the temperature and heat flux histories of the wall, the response factor expression takes the following form:

$$q''_{in}(t) = -\sum_{j=0}^{N_Z} Z_j T_{in,t-j\Delta t} - \sum_{j=0}^{N_Y} Y_j T_{out,t-j\Delta t} + \sum_{j=1}^{N_\varphi} \varphi_j q''_{in,t-j\Delta t} \quad (12)$$

In Equation 12, the terms Z, Y and φ represent the conduction transfer coefficients. While conduction transfer functions are rapid and convenient for whole building energy simulation, they cannot be used directly in the simulation of surfaces with variable thermal properties. Barbour & Hittle (2006) pre-calculated extra sets of conduction transfer functions to handle variable properties. The number of extra sets ranged from 3 to 599,999 to achieve proper accuracy. The computational cost associated with the higher sets of transfer functions limits the application of such methods in whole building energy simulation. Even with these disadvantages, the transfer function approach is still the most widely used approach in whole building energy simulation, due to the simplicity and computation speed. To ensure maximum applicability, any transient conduction model may be employed and be coupled with the ground domain. For the current work, the transfer function approach was utilized.

The exterior of the zone surface (T_{out} in Equation 12) is then coupled to the ground domain. This is performed using a convective boundary with a large value of surface conductance. This essentially becomes a temperature boundary on the surface. The ground domain supplies the surface heat balance with an average temperature for transient surface conduction calculations, and in return the surface heat balance supplies the ground domain with an average heat flux. The ground domain uses this heat flux as the boundary for cells adjacent to the surface. The

basement wall and floor are treated as separate boundary condition surfaces, by both the zone and the ground models.

Integration of the ground domain and the zone heat balance occurs at the surface exterior. Other possibilities exist, such as including the zone surface directly in the ground model domain. The coupling to the zone air heat balance would then occur at the convective boundary between the zone air and the wall interior surface. Allowing the surface heat balance manager to simulate the wall itself allows the wall solution type to be separate from the ground model. The wall may then be simulated using transfer functions or a finite difference approach, and could contain variable properties or other specialized features.

The ground domain is simulated at the time step of the air and fluid system simulation. The zone and surface heat balance equations occur at a different time step. Thus, the boundary conditions imposed on the ground domain are constant during all ground time steps until the next surface time step. When the surface begins a new time step, the aggregated energy added by the ground domain over the previous time step is used as the boundary. Since the integration occurs at the exterior surface of the domain, and the zone typically runs at time steps less than one hour, the lag will be insignificant over the course of a long-term simulation. Very light-weight surfaces may be more prone to inaccuracy with this assumption, however this effect is further dampened if the zone is well-controlled, such that the inside temperature is nearly constant.

Ground Domain Boundary Conditions

A Dirichlet condition $\left(T = T\left(z,\ t\right)\right)$ is applied on the ground domain at the far-field faces, which includes the bottom face of the calculation domain. In this model, cell centroids are not

aligned directly at the outer boundary surface, so the far-field temperature is applied to the outer surface of the cell. An energy balance is evaluated on the cell to determine a centroid cell temperature. The boundary temperature is calculated at a given time and depth using a standard expression introduced by Kusuda & Achenbach (1965):

$$T\left(z,t\right)=\overline{T_s}-\overline{\Delta T_s}exp\left(-z\sqrt{\frac{\pi}{\alpha t}}\right)cos\left(\frac{2\pi t}{\tau}-z\sqrt{\frac{\pi}{\alpha t}}-\theta\right) \tag{13}$$

Three parameters, $\left\{\overline{T_s},\overline{\Delta T_s},\ \theta\right\}$, must be estimated from knowledge of the ground temperature variation, either approximated from weather or location data, or generated from experimental ground temperature data.

The ground surface energy balance includes convective heat transfer as well as radiation and evapotranspiration on the exterior surface, with conduction to the interior of the domain. Evapotranspiration is modeled using the approach presented by Allen, et al. (1998), which governs the rate of evapotranspiration according to:

$$h_{fg}E=\frac{\delta\left(G_r-G_s\right)+\frac{\rho_a C_{p,a}e^{'}}{R_{aero}}}{\delta+\gamma\left(1+\frac{R_s}{R_{aero}}\right)} \tag{14}$$

Solution Algorithm

The ground domain is solved with an inherently stable implicit numerical formulation to ensure robustness within the variable time step environment. The system of equations is solved via iteration. Initialization of the domain is performed using a thermal gradient in the domain according to the far-field boundary specification. Convergence of the iteration is determined by

a specified maximum absolute temperature change in the domain. For the cases described in this work, a value of 0.005°C (0.009°F) was utilized, although the final implementation of the model allows refined control over convergence of different aspects of the domain.

The integration between simulation domains adds complexity to the solution scheme for the model. As already mentioned, the zone heat balance occurs at a time step larger than the ground model, so that the effects are lagged between the two domains. In addition, the fluid loop solver is an iterative quasi-steady solution that can both vary the time step and back step within the main iteration loop. It is expected that the ground domain will respond fastest in the near pipe region, where temperatures could rapidly change based on loop conditions. Because of this, the ground domain thermal network is updated at variable time steps, aiding in a lightweight computational burden by not simulating the ground at each iteration. The overall time step operation and model calling points are shown in Figure 5. The ground domain is updated on the first system time step, while the fluid circuit is shown to be embedded inside the system time integration loop. Figure 5 also shows that the surface temperatures are updated at a higher level, resulting in a lag of information transfer between the domains.

Model Evaluation

Foundation heat exchangers (Spitler, et al. 2010) are a special type of ground heat exchanger placed in the excavation area of a basement. This placement results in significant thermal interaction with the zone. Multiple buried pipes can be laid in this same trench, which results in significant thermal interaction between pipes. These interactions, along with the relatively close proximity to the ground surface result in a lower heat exchanger capacity per length compared to vertical borehole heat exchangers, which interact with the nearly constant deep ground

temperature. For traditional building design, foundation heat exchangers do not provide sufficient capacity, but low-energy designs with lower peak loads can make use of these in some climates and configurations (Cullin, et al. 2012).

Experimental Facility

The foundation heat exchanger configuration provides a useful validation configuration for this modeling work as it includes high thermal activity between multiple pipes and between the ground and zone. An experimental facility in Oak Ridge, TN, USA (as described by Xing, et al. 2011)) consisted of a full scale low-energy residential building with a foundation heat exchanger and a multiple pipe horizontal heat exchanger in a utility trench. A photo of this piping is shown in Figure 6a, with a simplified schematic of the foundation heat exchanger in Figure 6b. These two figures show how the tubing is laid directly into the already excavated areas. This reduces or eliminates the cost of drilling and excavation work that is done specifically for heat exchanger installation.

The fluid loop, as installed at the experimental facility, is shown in Figure 7a. The foundation heat exchanger section of the fluid loop was 36.8 m (120.7 ft) for each tube, and there were six tubes in the heat exchanger. The tube burial location (both depth and distance from basement wall) varied, as the excavation was not uniform. For the purpose of this study, the tube closest to the ground surface was assumed buried 0.31 m (1 ft) deep and 1.67 m (5.5 ft) away from the basement wall. The tube closest to the basement wall was assumed buried 1.52 m (5 ft) deep and 0.61 m (2 ft) from the basement wall. There was also a conventional earth heat exchanger with a configuration similar to the foundation heat exchanger, located away from the basement, with each pipe legnth of 54.6 m (179.1 ft). Undisturbed ground temperature was

measured away from(15) the heat exchanger installation. This data was used to perform parameter estimation to determine model parameters. Fluid temperature was measured at multiple locations around the loop. For the current validation efforts, only the loop inlet and outlet temperatures were utilized, for both component-model and system-level validation studies. Heat flux measurements were made along the basement wall at multiple depths, characterizing the effects of the heat exchanger on the zone. This heat flux data was used in validating the integration of the ground model with the zone heat balance.

EnergyPlus Model

The model was implemented in the whole building energy simulation software EnergyPlus (Crawley, et al. 2001) as a new component in the central plant simulation algorithms. The fluid loop in the experimental facility (Figure 7a) consists of a foundation heat exchanger region near the basement as well as conventional heat exchangers, some of which pass through a rain garden area. In EnergyPlus, the system was modeled as two heat exchangers: the foundation heat exchanger, and the remainder of the system as a single horizontal heat exchanger, shown in Figure 7b. To complete the full system simulation in EnergyPlus, a load profile object was utilized to provide heat input to the loop, and an idealized pump was added to provide flow to the system. Experimental measurements of system flow rate were used as a boundary condition on the model.

For component-model validation, the model directly used the experimental data for entering temperature and flow rate, overriding any system effects, in order to isolate the validation to the component itself. In Figure 7b, point A represents the point where experimental temperature was

applied. For system simulation validation, the component directly used the conditions entering from upstream components.

During these studies, the model algorithms were optimized for improved computational efficiency. Performing an annual detailed foundation heat exchanger simulation within the EnergyPlus whole building shell using a fully optimized version of the application took less than five minutes on a modern computer. This computational burden is within acceptable levels for whole building energy simulation.

Numerical Considerations

Grid independence testing traditionally consists of running with an increasingly denser mesh until a convergence criterion is achieved, usually a maximum temperature differential in the domain between iterations. A feature of the current model is the level of integration between the ground, zone and fluid systems. This integration provides the ability to use grid independence metrics beyond domain temperatures. Implemented within a whole building energy simulation environment, the effects on zone and the fluid system provides more relevant metrics. The grid independence study focuses on fluid and ground temperatures, but also includes the effects on zone loads, which directly impact energy use. The whole building simulation environment also requires a model that is computationally efficient. A typical grid independence analysis will produce a fully independent grid, but at the cost of an unusable grid configuration. This grid independence study balances computation and accuracy, with a focus on building energy use as a metric.

Numerical Considerations: Preliminary Discussion

The grid independence study was performed varying the grid using three mesh density parameters, each of which has a distinct effect on the accuracy and computational burden of the domain:

- Cartesian Inter-Partition Mesh Density (X and Y directions treated equally in this study)
- Axial Mesh Count
- Radial Soil Mesh Count

Trials were made of each mesh parameter at the values: {1, 4, 7, 10} (64 total). The output metrics for this integrated model include the heat exchanger outlet temperature, spatially averaged basement wall temperature, and basement zone load. Each of these are averaged for an annual simulation to provide a single metric for the entire annual run.

- **XY Mesh Density** The XY mesh density is used to define the number of cells between each partition or surface in the domain. A value of one means that a single Cartesian cell is placed between any two partitions, resulting in a highly coarse domain. This parameter refines the mesh near the zone surfaces.
- **Axial Mesh Count** Axial mesh count is the number of cells along the length of the pipe segments placed in the domain. With a single cell, the effects of temperature non-linearity cannot be captured. The effects of fluid temperature variation along the pipe length is captured with a higher number of axial cells.
- **Radial Mesh Count** The radial mesh count is the number of radial soil cells inside a Cartesian cell containing a pipe. Using a single radial cell can provide suitable accuracy because the Cartesian cell will also contain an interface cell, a pipe wall cell, and a fluid cell.

Even with a single radial cell, the near-pipe region is refined relative to the Cartesian system. The addition of radial cells is expected to have minimal impact on results.

- **Overall Mesh Count** The overall mesh count is a function of the three interacting mesh parameters. An increase in axial cell count increases the number of cells in the domain linearly, as it is adding domain cross sections. An increase in XY mesh or radial mesh count is dependent on the number of features in the domain. The interactions between each parameter are non-trivial, having effects on computation time, accuracy, and convergence.

Numerical Considerations: Computation Time

The computation time results are shown in Figure 8 as a function of overall mesh count. As expected the computation time trend was to rise as the total number of cells increases. However, the curve is not monotonically increasing. The total cell count obscures the interactions between the mesh parameters. This is explained by example: The total cell count may increase as a combined result of increasing the radial count and reducing the axial count. The computation cost of additional radial cells is smaller than additional axial cells, thus the computation time can decrease even with an increase in overall cell count. As a reference, the total cell count for the configuration used in further experimental validation is labeled on the plot.

Numerical Considerations: Grid Independence

The grid independence study showed that the radial mesh count is relatively insignificant; the XY mesh can provide independence at a low level, whereas the axial mesh count is a major factor. The axial mesh parameter minimum value was therefore set at four. Each of the three output metrics (heat exchanger outlet temperature, basement wall temperature, and basement

load) are displayed in Figure 9. The data is presented for each metric with three curves. The three curves represent varying a single mesh parameter while the other parameters remain refined at the maximum mesh density value. This isolates the effect to the single parameter being swept.

For the heat exchanger outlet temperature (Figure 9a), the XY mesh shows a change of nearly 1.7°C (3.0°F) from a single mesh value to the next, but the effects diminish with a coarse grid. The effects of axial and radial mesh parameters provided less than a 0.25°C (0.45°F) change across the variation of parameters. This confirms the expectation that a single radial cell suffices, while values less than 4 for XY and axial mesh parameters provide independence.

For the basement wall temperature (Figure 9b) and basement zone load (Figure 9c), the radial and XY mesh parameters are insignificant, showing less than a 10% change throughout the parameter variation. The axial effect is more pronounced, showing variation yet trending toward convergence as the number of axial cells is increased. Since the axial effect did not have an effect on fluid temperature, this indicates that the axial parameter has more effect on the near-zone region, allowing ground temperature variation to be included.

Numerical Considerations: Discussion

The results of this study were used to guide the selection of model grid parameters for experimental validation. The model showed greater sensitivity to the axial mesh count than the other mesh parameters. The selected values for XY and radial mesh count was 3, while the axial mesh count was more increased to 12. This value results in a grid where each cell is 3.07 m (10.07 ft) long in the axial direction. Using the coarse grid for XY and radial mesh parameters, while using a refined axial grid results in the computation time displayed on Figure 8. This very

low computation time is achieved while still producing a high level of accuracy, as demonstrated by further validation in the following sections. Larger values of each parameter could have been selected for experimental validation, however this would result in an increase in computation time and put the model in conditions that may not be feasible for the simulation of systems in practice.

Analytic Validation of Interface Cell

The approach used to model the near-pipe region utilizes a coordinate system interface cell to provide thermal interaction between the two coordinate systems. The energy balance approach used in developing the system of equations to solve the system ensures that under the given assumptions, energy will be conserved. However, the effects of certain assumptions used in developing the interface cell must be validated to ensure the coordinate system mapping can produce suitable accuracy. These assumptions include:

1. The interface cell is spatially isothermal and for the purpose of the thermal network is located at a midpoint of the interface cell straight side, as per Figure 3d.
2. The heat transfer between the interface and the inner radial system is one dimensional and driven by the distance between the outermost radial centroid and the midpoint of the side of the interface cell.
3. The heat transfer between the interface and outer cells is rectilinear and driven by the distance between the Cartesian cell centroid and the midpoint of the side of the interface cell.

In order to validate this approach, the pipe was approximated as a line source in an isotropic domain. The idealized simulation domain was constructed with the following properties:

- A single small pipe, centered in the domain
- Domain size » pipe size
- Constant ground surface and far-field boundaries (T=0°C (32°F))
- Disabled dynamic properties (constant specific heat)
- Initialization of domain at (T=0°C (32°F))
- Pipe cell bypassed any fluid flow, a constant heat gain was added to the domain at the pipe wall

In this way, the small pipe approximated a line source in an isotropic domain. This idealization modified the domain boundaries (including the fluid boundary) but left the coordinate system interface treatment unmodified. The analytic solution for the idealized situation was described by Ingersoll & Plass (1948):

$$T(r,t) = T_0 + \frac{Q'}{2\pi kt}\int_X^\infty \frac{e^{\beta^2}}{\beta} d\beta \qquad (16)$$

Where β is simply an integration variable, and the integral domain limit X is a normalized radius:

$$X = \frac{r}{2\sqrt{\alpha_s t}} \qquad (17)$$

The numerical model and the analytic solution were sampled at two radial points, both of which were outside of the interface, in the Cartesian domain. One point was close to the interface, at a distance of 0.056 m (0.183 ft), while the other point was 0.556 m (1.824 ft) away. The results are shown in Figure 10. The simulation domain matched well with the analytic solution, with a peak absolute error of 0.09°C (0.16°F). This peak error occurred at the cell

nearest the pipe at the initial time step, with the error diminishing rapidly in both time and space away from this point. This is attributed predominantly to the differences between the analytic solution assumptions and the actual model; the pipe was not actually a line source, but rather a small cylinder in the domain.

Undisturbed Ground Temperature

Undisturbed ground temperature was measured at the experimental facility at five depths: 0.3 m (1 ft), 0.6 m (2 ft), 0.9 m (3 ft), 1.5 m (5 ft) and 1.8 m (6 ft). At the shallowest measurement, the ground temperature is strongly dependent on surface conditions such as solar gain, evapotranspiration, and convection to outdoor air. As the depth increases, the temperature becomes less dependent on surface effects, and more dependent on deep ground effects. In terms of simulation, these include the selection of far-field boundary condition models and parameters.

Parameter estimation was performed using this experimental data to optimize simulation parameters. A cyclic heuristic direct search algorithm was employed where the objective function was the sum of the squared error between experimental and model data. This algorithm is robust if given a valid starting point for the optimization. The decision variables in the study were the ground density and specific heat, and the far-field temperature specification parameters $\left(\bar{T}_s,\ \overline{\Delta T_s}\right)$. The feasible ranges on the parameters are approximately 20% of the initial starting point. The initial starting point for thermal properties of the soil are based on a clay loam soil with water content as described by Lamberg, Lehtiniemi, & Henell (2004). The initial starting point for temperature data is approximated from measured weather data. The parameter estimation procedure provided the values shown in Table 1.

Using these optimized parameters, the undisturbed ground temperature was predicted by the simulation model without any pipes in the domain. The results for three representative depths are shown in Figure 11. The mean bias error over the entire data set was 0.36°C (0.65°F).

At greater depths, the model deviated more from the experimental measurements than at the shallower depths. A possible source of error is the far-field boundary temperature formulation (Kusuda & Achenbach 1965). This form of the boundary condition may not capture all of the boundary effects that may exist in the experimental data, including:

- Unusual variation in seasonal temperature variation in the previous year(s)
- Non-isotropic ground, perhaps layers of different ground materials
- Proximity to underground water table and ground water flow
- Other experimental artifacts (ground not actually *undisturbed*)

Component-level Validation

Component model validation was completed to demonstrate the model's ability to predict outlet conditions provided a tightly bounded solution domain. The entering fluid temperature was fixed at each time step to experimentally measured heat exchanger inlet temperature, which ensured that over the course of the simulation, the error in total heat transfer to the ground was minimized. With an accurate experimental temperature entering the heat exchanger throughout the simulation, the error in the amount of heat transfer into the ground was minimized, and the boundary condition for the fluid remained accurate and did not drift from the experimental conditions.

The simulated heat exchanger outlet temperature matched experimental data with a mean error of 0.3°C (0.54°F). The quality of the component-model validation is better represented with the magnitude of the temperature change across the heat exchanger, or heat transfer rate. Assuming a constant specific heat, this was calculated as:

$$\dot{q} = \dot{m} C_p \left(T_{out} - T_{in} \right) \tag{18}$$

The resulting heat transfer rate is shown in Figure 12. With a tightly controlled (fixed inlet) simulation, the predicted heat transfer rate matched the experimental data with a mean bias error of 27.5 W (93.8 btu/hr). The model predicted individual peaks of heat transfer rate with good accuracy aside from deviations in the initial and peak heat rejection periods. The deviation in the initial period is possibly due to the initialization of the ground domain, which may be significantly different from that found at the experimental site in the back-filled soil. The undisturbed ground temperature prediction also could not match experimental measurements in the peak heat rejection period. The error in heat transfer rate prediction in this region is expected to be due to this effect, which may be manifested as an error in thermal properties or boundary parameters.

System-level Validation

For system simulation, the load on the heat exchangers was calculated from experimental data, and used as a boundary for a full loop simulation. This type of validation is a more exacting test than the component-level validation because the boundary conditions on the fluid thermal network are not at the inlet of the heat exchanger model, rather they exist as boundary

conditions on the fluid loop. Any inaccuracy in heat transfer from the fluid to the ground affects the fluid response in subsequent time steps.

The heat pump entering fluid temperature (same as heat exchanger outlet temperature within the simulation model) is shown in Figure 13. The mean bias error in outlet temperature prediction was 1.3°C (2.3°F). The model showed less accuracy predicting temperatures beginning near hour 6500 when the system was off-line periodically. When there is no flow in the system, the fluid temperature is predicted using a simplified natural convection approach. As shown in Figure 14, the model tends to under predict these periods. Once flow is restarted, the fluid heat transfer is governed by the loads in the system and the forced convection model.

Basement Wall Heat Flux

The experimentally measured data at the foundation heat exchanger test site includes basement wall heat flux data. For foundation heat exchangers specifically, the thermal exchange with the zone is an important design parameter. The proximity of the heat exchanger pipes has a significant impact on the zone loads and the zone conditions. In EnergyPlus, building surfaces (walls) are defined as single objects, modeled with one-dimensional transient conduction. Accordingly, for this validation the basement floor and wall were single surfaces.

Wall heat flux was measured experimentally at three locations along the basement wall [depths = 0.36 m (1.17 ft), 1.07 m (3.5 ft) and 1.73 m (3.5 ft)]. An area-weighted averaging scheme was used to regress these experimental values into a single representative wall heat flux measure. Based on the measurement spacing, measurement #1 has a weight of 0.28, measurement #2 has 0.27, and measurement #3 has 0.45. The resulting average measured wall heat flux was compared to the simulation wall heat flux for the entire surface, as shown in Figure

14. The overall trend and peak heat transfer was predicted by the model with an average annual absolute error between the model and experimental data of 1.1 W/m^2 (0.35 $btu/hr\text{-}ft^2$). The model shows higher fluctuations, which represents a higher sensitivity to the ground surface phenomena than the experimental top measurement value.

Acknowledgments

<acknowledgements removed>

Conclusions/Future Work

A generalized horizontal ground heat exchanger model has been developed which integrates systems within a whole building energy simulation environment. The model uses a coarse grid three-dimensional Cartesian coordinate system as the basis for a numerical solution, with the near pipe regions meshed using a secondary radial coordinate system. This approach provides a refined grid in the near pipe region, and is generalized to allow any number of pipes to be placed in the domain. Fluid flow in the pipe is simulated in a flow-wise fashion as it circuits through the domain to capture interference effects of multiple pipes and flow direction.

The model is integrated with the zone heat balance through a boundary condition at the zone exterior surface. The model is also coupled to the hydronic system simulation through the fluid inlet and outlet of each fluid circuit in the model. These integrations allow the same mass of ground to interact thermally with the zone and the ground heat exchanger that may be serving the zone. This allows for studies of near-zone heat exchangers with improved accuracy over decoupled approaches. The model provides suitable accuracy with a coarse grid when validating against experimental measurements. Heat exchanger exiting fluid temperature is predicted with

a mean bias error of 1.3°C (2.3°F). Average annual basement wall heat flux is predicted to 1.1 W/m2 (0.35 btu/hr-ft2).

Future work for the model includes a more advanced treatment of the far-field boundary specification. A modified form of this may allow for an improved parameter estimation of ground properties against undisturbed ground temperature data and an overall improvement in accuracy. The treatment of the fluid in the pipe during offline times could also be enhanced as the temperature prediction deviates during this time when natural convection dominates the fluid.

Nomenclature

Variables

A	Surface area
C_p	Specific heat
e'	Vapor pressure deficit of the air
E	Rate of evapotranspiration from the surface
G_r	Net radiation into the surface
G_s	Soil heat flux from the surface
h	Convection coefficient
h_{fg}	Latent heat of vaporization
k	Thermal Conductivity
m	Mass
$\dot{m}$	Mass flow rate

N	Number or count of a material or property
Nu	Nusselt Number
Pr	Prandtl Number
$\dot{q}$	heat transfer rate
Q'	Line source heat intensity per unit length
q''	Heat flux
R	Thermal Resistance
Re	Reynolds Number
T	Temperature
t	Time
$\overline{T_s}$	Annual average surface temperature
U	Overall surface conductance
V	Volume
z	Depth from Ground Surface

Greek Letters

α	Thermal diffusivity
γ	Psychrometric constant
δ	Slope of the saturation vapour pressure temperature relationship
$\overline{\Delta T_s}$	Average amplitude of surface temperature
Δx	Cell or domain length dimension
Δy	Same as Δx

ζ	Geometric series coefficient
θ	Phase Shift for minimum ground surface temperature
ρ	Density
τ	Coefficient to normalize units of time
Subscripts	
0	Initial condition
a	Property of the air
aero	Aerodynamic Property
c	Radial centroid
D	Dimensionless based on pipe diameter
f	Property of the fluid
i, j	Arbitrary index
in	Process into a cell or region of interest, or a property of a surface interior
o	Outer radius
out	Process out of a cell or region of interest, or a property of a surface exterior
region	Property of an inter-partition mesh region
s	Property of a surface

References

Adjali, M., Davies, M., & Rees, S. 2004. A comparative study of design guide calculations and measured heat loss through the ground. *Building and Environment, 39*(11):1301-1311.

Allen, R. G., Pereira, L. S., Raes, D., & Smith, M. 1998. *Crop Evapotranspiration - Guidelines for computing crop water requirements.* Food and Agriculture Organization of the United Nations.

Andolsun, S., Culp, C. H., & Haberl, J. 2010. EnergyPlus vs DOE-2: The Effect of Ground Coupling on Heating and Cooling Energy Consumption of a Slab-on-Grade Code House in a Cold Climate. *Proceedings of SimBuild 2010.*

Austin, W., Yavuzturk, C., & Spitler, J. D. 2000. Development of an In-Situ System and Analysis Procedure for Measuring Ground Thermal Properties. *ASHRAE Transactions, 106*(1):365-379.

Barbour, J. P., & Hittle, D. C. 2006. Modeling Phase Change Materials With Conduction Transfer Functions for Passive Solar Applications. *Journal of Solar Energy Engineering, 128*(1):58-68.

Bau, H. H., & Sadhai, S. S. 1982. Heat losses from a fluid flowing in a buried pipe. *International Journal of Heat and Mass Transfer, 25*(11):1621-1629.

Binks, J. 2011. Closing the Loop: Office Tower Simulation Assumptions vs Reality. *Proceedings of Building Simulation 2011,* 941-948.

Bronfenbrener, L., & Korin, E. 1999. Thawing and refreezing around a buried pipe. *Chemical Engineering and Processing, 38*(3):239-247.

Chengju, H., Changsheng, G., & Kai, X. 2012. Random Heat Temperature Field Model Analysis on Buried Pipe of Ground Source Heat Pump. *Advanced Materials Research, 383*:6626-6631.

Chung, M., Jung, P.-S., & Rangel, R. H. 1999. Semi-analytical solution for heat transfer from a buried pipe with convection on the exposed surface. *International Journal of Heat and Mass Transfer, 42*(20):3771-3786.

Claesson, J. & Dunand, A. 1983. Heat Extraction from the Ground by Horizontal Pipes – A Mathematical Analysis. Department of Mathematical Physics, Lunds University, Sweden.

Claesson, J., & Hagentoft, C.-E. 1991. Heat Loss to the Ground from a Building - I. General Theory. *Building and Environment, 26*(2):195-208.

Crawley, D. B., Lawrie, L. K., Winkelmann, F. C., Buhl, W. F., Huang, Y. J., Pedersen, C. O., et al. 2001. EnergyPlus: creating a new-generation building energy simulation program. *Energy and Buildings, 33*(4):319-331.

Cullin, J. R., Spitler, J. D., Xing, L., Fisher, D. E., & Lee, E. S. 2012. Feasibility of Foundation Heat Exchangers for Residential Ground Source Heat Pump Systems in the United States. *ASHRAE Transactions, 118*(1), In Press.

Den, K. R., & Nielsen, E. 1998. Performance Prediction of a Sub-Slab Heat Exchanger for Geothermal Heat Pumps. *Journal of Solar Energy Engineering, 120*(4):282-288.

Dittus, P. W., & Boelter, L. M. 1930. *University of California Publications on Engineering, 2*:443.

Esen, H., Inalli, M., & Esen, M. 2007. Numerical and experimental analysis of a horizontal ground-coupled heat pump system. *Building and Environment, 42*(3):1126-1134.

Fan, D., Rees, S. J. & Spitler, J. D. 2012. A dynamic thermal network approach to the modelling of foundation heat exchangers. *Journal of Building Performance Simulation.* In Press.

Fisher, D. E., Rees, S. J., Padhmanabhan, S. K., & Murugappan, A. 2006. Implementation and Validation of Ground-Source Heat Pump System Models in an Integrated Building and System Simulation Environment. *HVAC&R Research.* 12(3a):693-710.

Ihm, P., & Krarti, M. 2004. Implementation of Two-Dimensional Foundation Model for Radiant Floors into EnergyPlus. *Proceedings of Simbuild 2004,* 1-12.

Ingersoll, L. R., & Plass, H. J. 1948. Theory of the ground pipe source for the heat pump. *ASHVE Transactions, 54*:339-348.

Kusuda, T., & Achenbach, P. 1965. *Earth Temperature and Thermal Diffusivity at Selected Stations in the United States.* Tech. rep., National Bureau of Standards.

Lamberg, P., Lehtiniemi, R., & Henell, A. M. 2004. Numerical and experimental investigation of melting and freezing processes in phase change material storage. *International Journal of Thermal Sciences, 43*(3):277-287.

Mei, V. 1988. Heat Pump Ground Coil Analysis with Thermal Interference. *Journal of Solar Energy Engineering, Transactions of the ASME, 110*(2):67-73.

Ngo, C. C., & Lai, F. C. 2005. Effects of Backfill on Heat Transfer From a Buried Pipe. *Journal of Heat Transfer, 127*(7):780-784.

Piechowski, M. 1996. *A Ground Coupled Heat Pump system with Energy Storage.* Ph.D. dissertation, Melbourne University.

Piechowski, M. 1999. Heat and mass transfer model of a ground heat exchanger: Theoretical development. *International Journal of Energy research, 23*(7):571-588.

Raymond, J., Therrien, R., Gosselin, L., & Lefebvre, R. 2011. Numerical analysis of thermal response tests with a groundwater flow and heat transfer model. *Renewable Energy, 36*(1):315-324.

Sadegh, A. M., Jiji, L. M., & Weinbaum, S. 1987. Boundary integral equation technique with application to freezing around a buried pipe. *International Journal of Heat and Mass Transfer, 30*(2):223-232.

Said, S. M., Habib, M., Mokheimer, E., Al-Shayea, N., & Sharqawi, M. 2009. Horizontal Ground Heat Exchanger Design for Ground-Coupled Heat Pumps. *Proceedings of Ecologic Vehicles and Renewable Energies*, 1-8.

Spitler, J., Xing, L., Cullin, J., Fisher, D., Shonder, J., & Im, P. 2010. Residential Ground Source Heat Pump Systems Utilizing Foundation Heat Exchangers. *Proceedings of Clima* 2010, Antalya Turkey.

Stocki, M., Curcija, D. C., & Bhandari, M. S. 2007. The Development of Standardized Whole-Building Simulation Assumptions for Energy Analysis for a Set of Commercial Buildings. *ASHRAE Transactions, 113*(2):422-435.

Thomas, H. R., & Rees, S. W. 2009. Measured and Simulated Heat Transfer to Foundation Soils. *Geotechnique, 59*(4):365-375.

Tobias, J. R. 1973. Simplified Transfer Function for Temperature Response of Fluids Flowing through Coils, Pipes or Ducts. *ASHRAE Transactions, 79*(2):19-22.

Xing, L., Cullin, J. R., Spitler, J. D., Im, P., & Fisher, D. E. 2011. Foundation Heat Exchangers for Residential Ground Source Heat Pump Systems--Numerical Modeling and Experimental Validation. *HVAC&R Research, 17*(6):1059-1074.

Yavuzturk, C., & Spitler, J. D. 1999. A Short Time Step Response Factor Model for Vertical Ground Loop Heat Exchangers. *ASHRAE Transactions, 105*(2):475-485.

Tables

Table 1: Parameters from optimization against experimental undisturbed ground

Parameter Name	Symbol	Value	Units	Value	Units
Ground Density	ρ	852.3	Kg/m3	53.2	lb/ft3
Ground Specific Heat	C	2073.8	J/kgK	0.49	btu/lb°
Average Annual Surface Temperature	$\bar{T}$	12.86	°C	55.16	°F
Average Amplitude of Surface Temperature	$\overline{\Delta T}$	13.73	°C	24.71	°F

Figure 1: One possible simulation domain that includes heat exchanger pipes and a basement zone

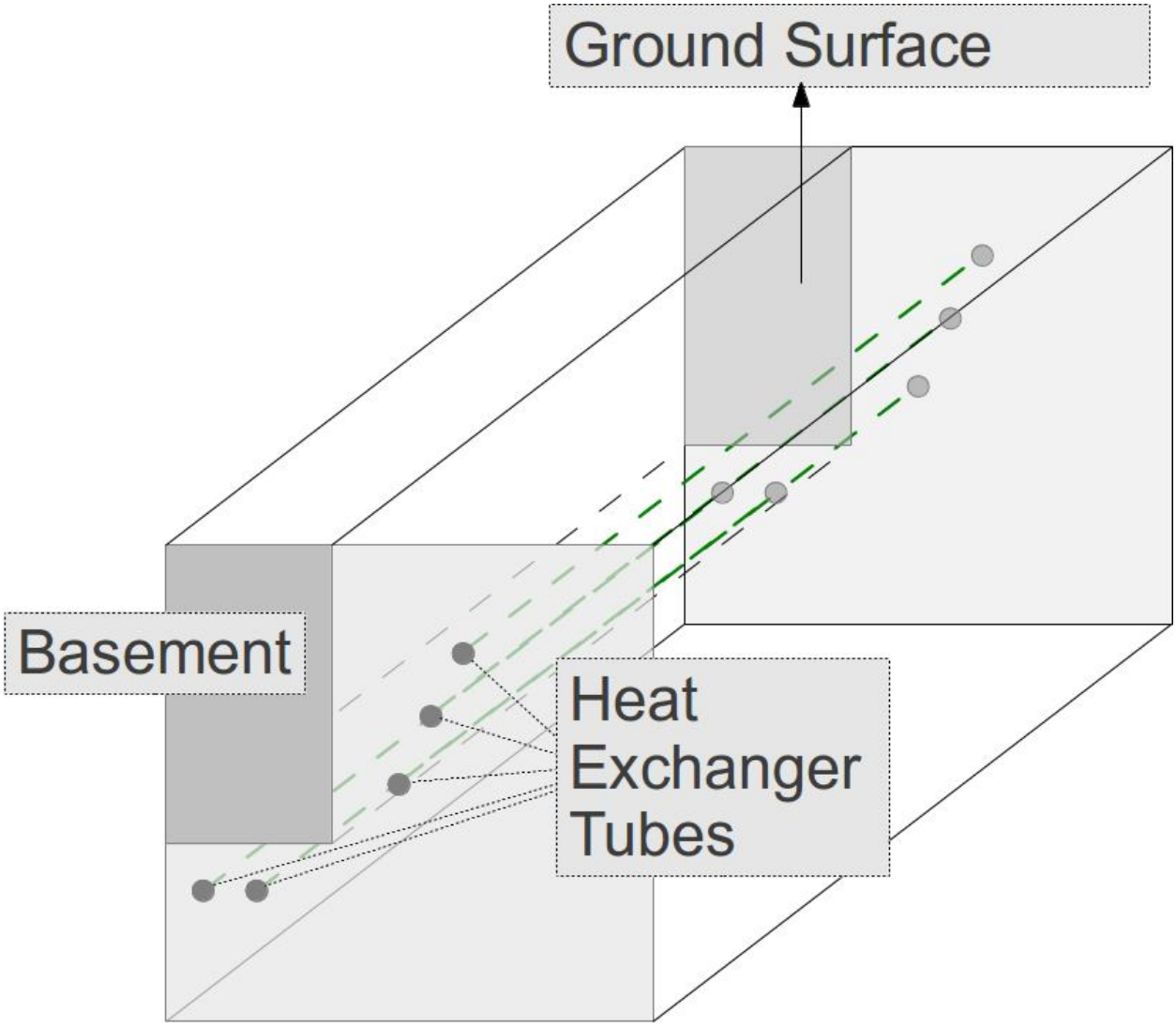

Figure 2: Domain visualization for the partition based mesh development procedure

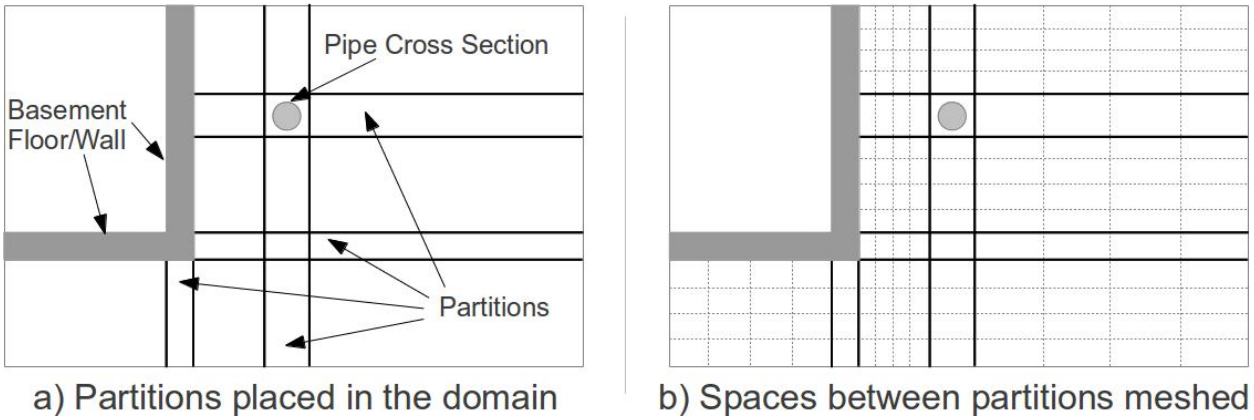

Figure 3: Approaches to simulate pipe cell effects within a Cartesian coordinate system domain

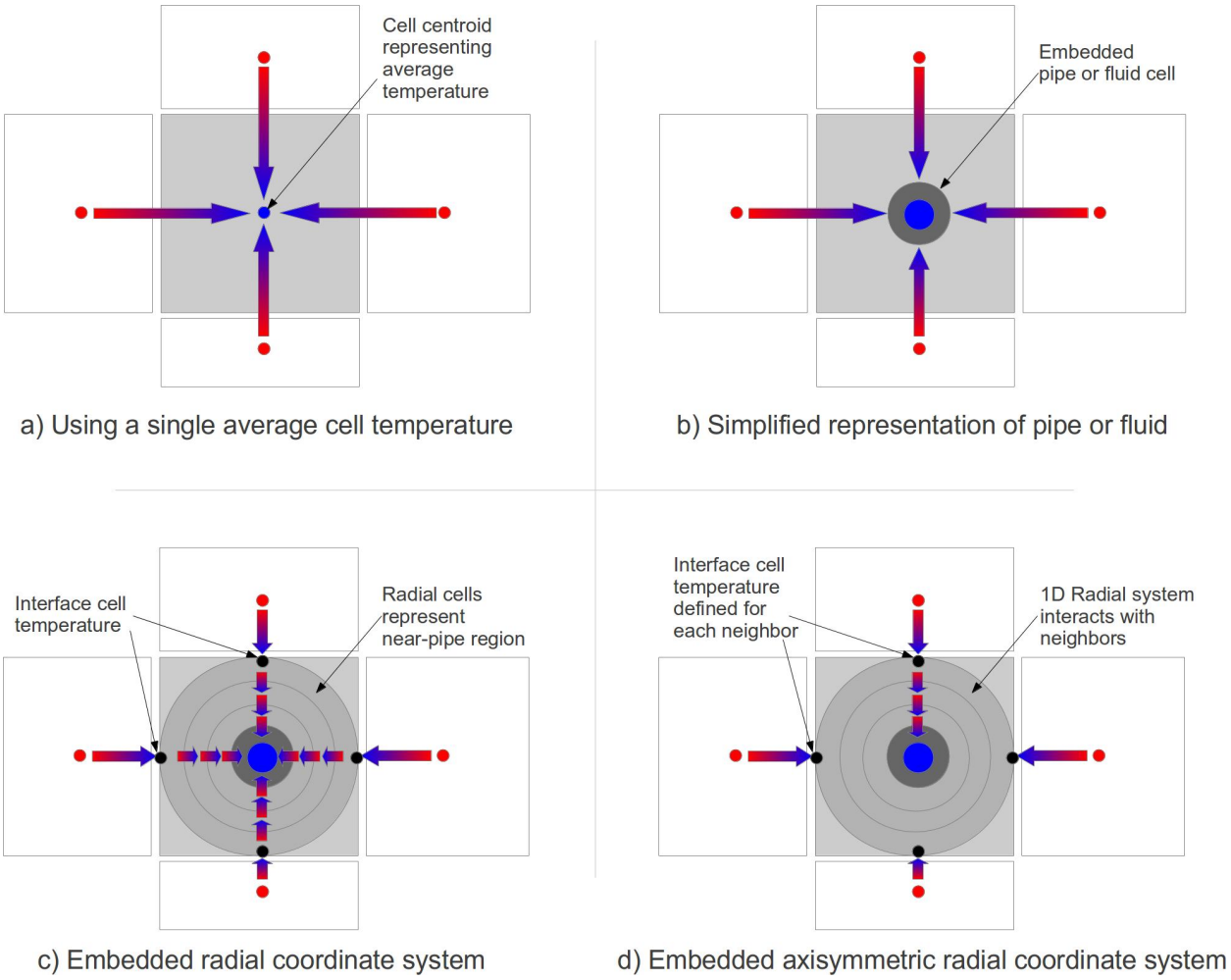

Figure 4: 2D and 3D representations of the fluid cell, with radial coordinate system nomenclature

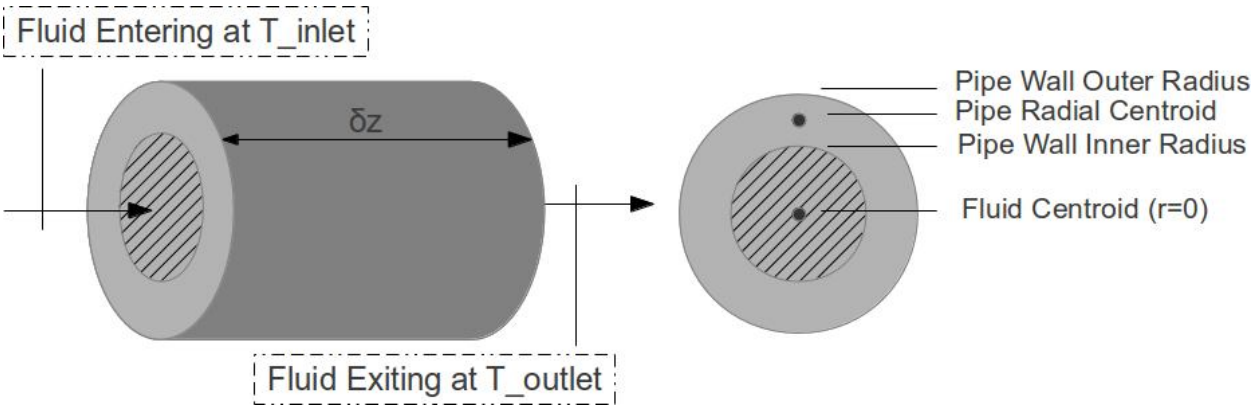

Figure 5: Solution logic of integrated modeling system, showing relevant variable calculation points

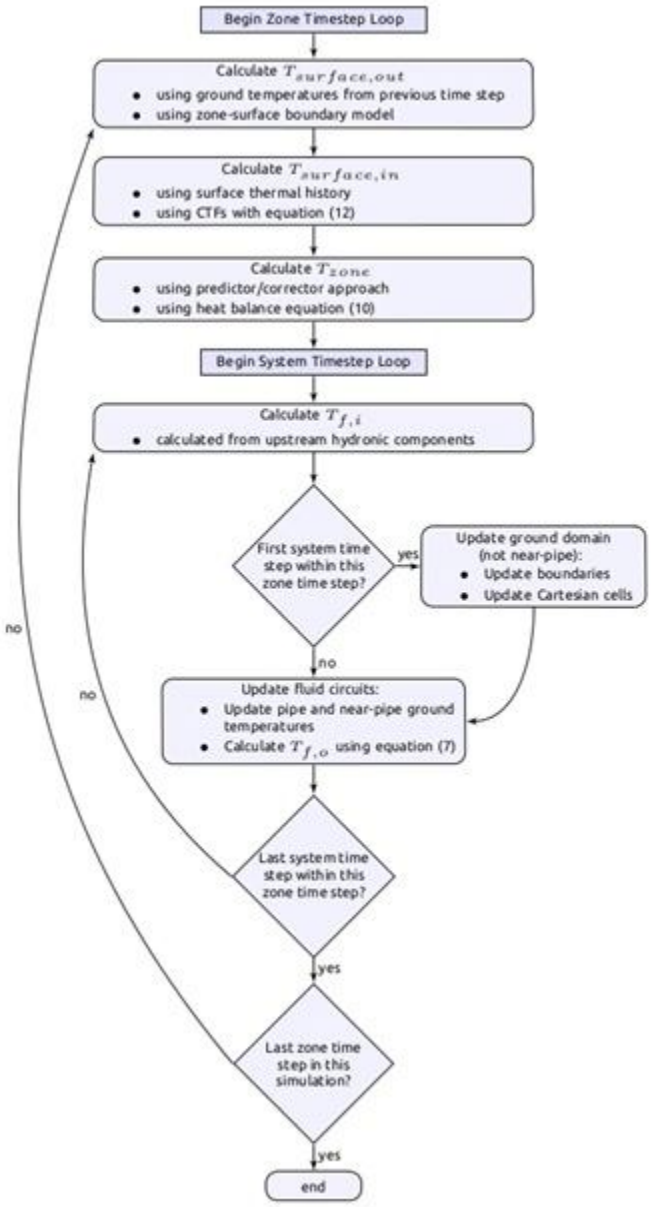

Figure 6: Foundation heat exchanger installation and representation of thermal interaction

a) Photo of experimental facility (Courtesy of Piljae Im. Used by permission.)

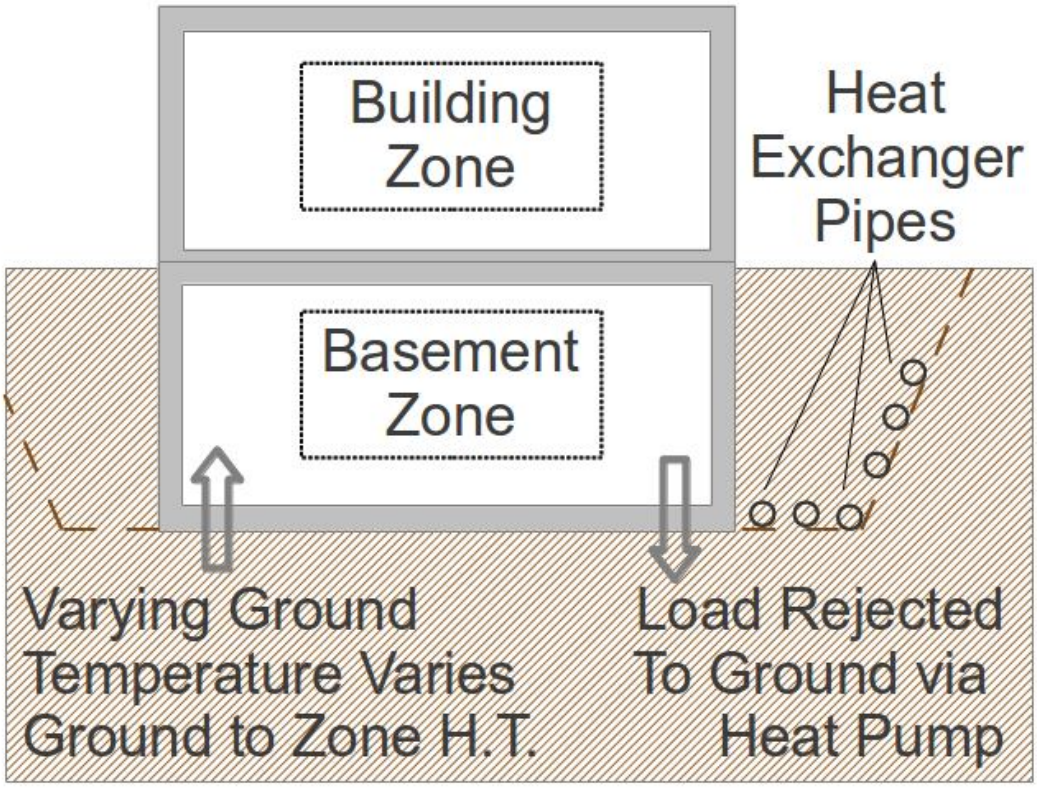

b) Simplified schematic

Figure 7: Experimental fluid loop and the simplified representation used in validation efforts

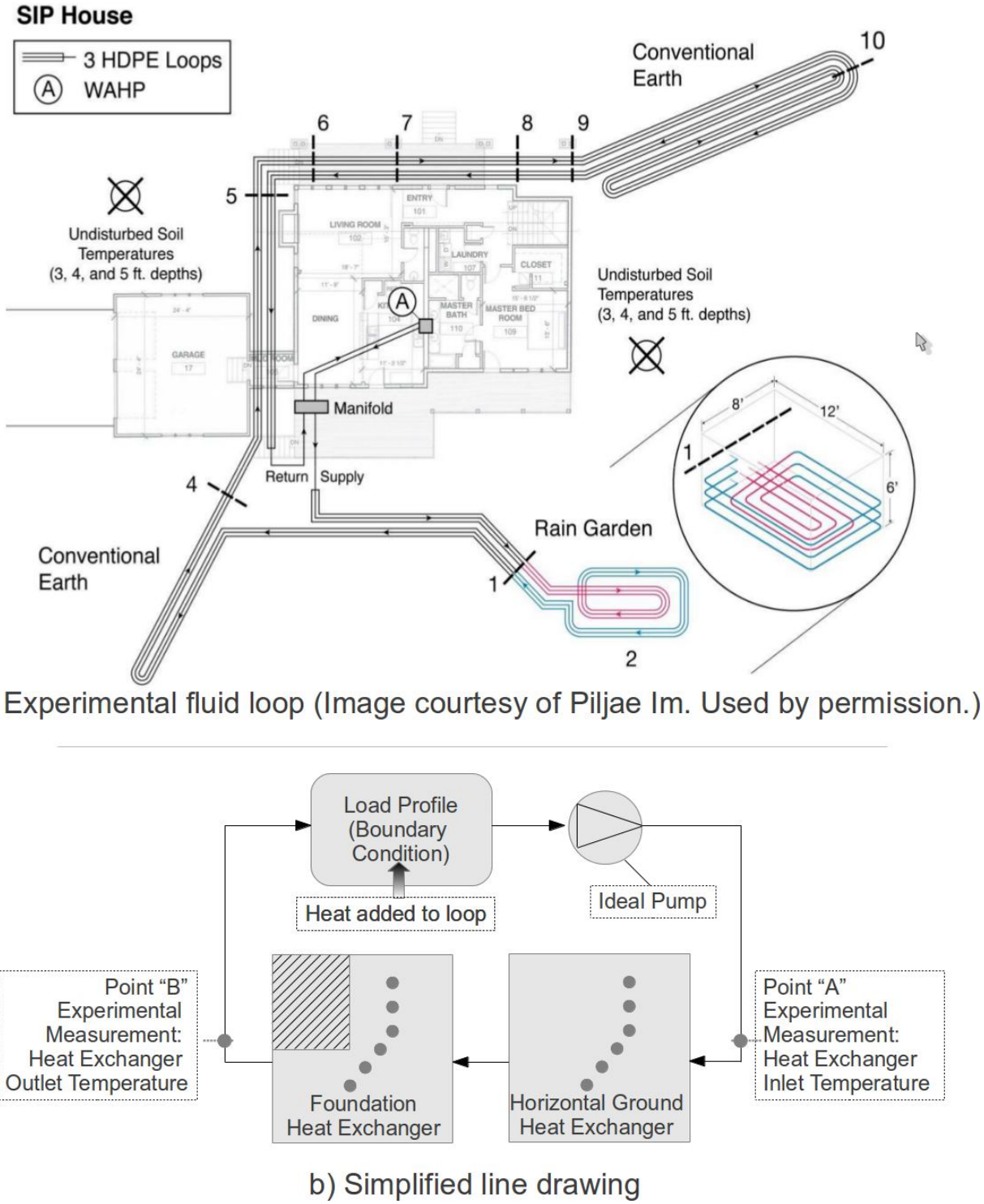

Figure 8: Overview of computation time increase as a function of the total number of cells in the

domain

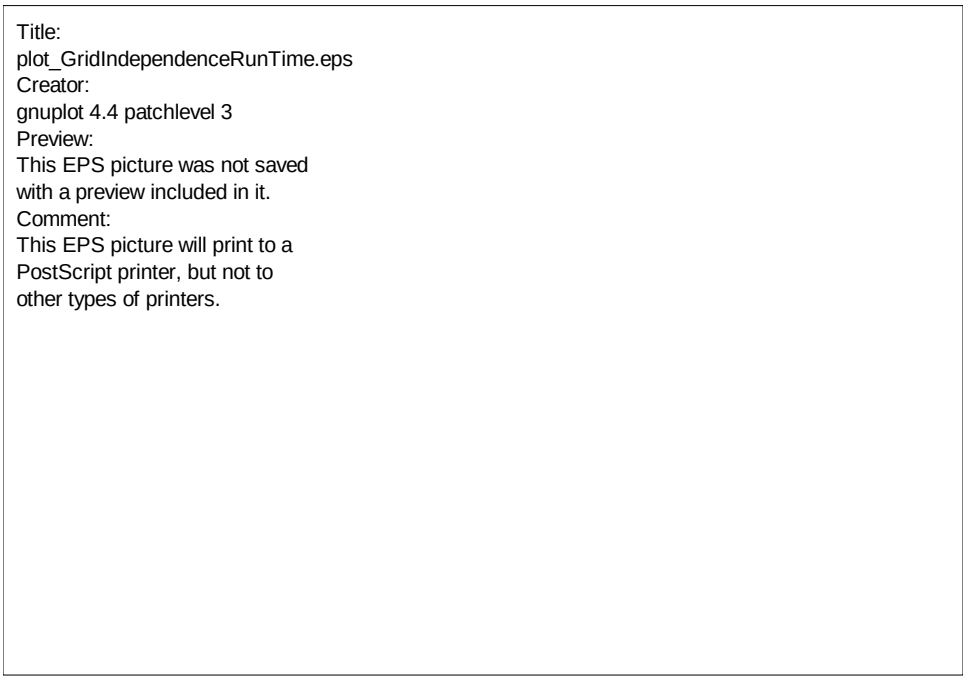

Figure 9: Grid independence results: value of a domain property as a function of varying each mesh parameter separately

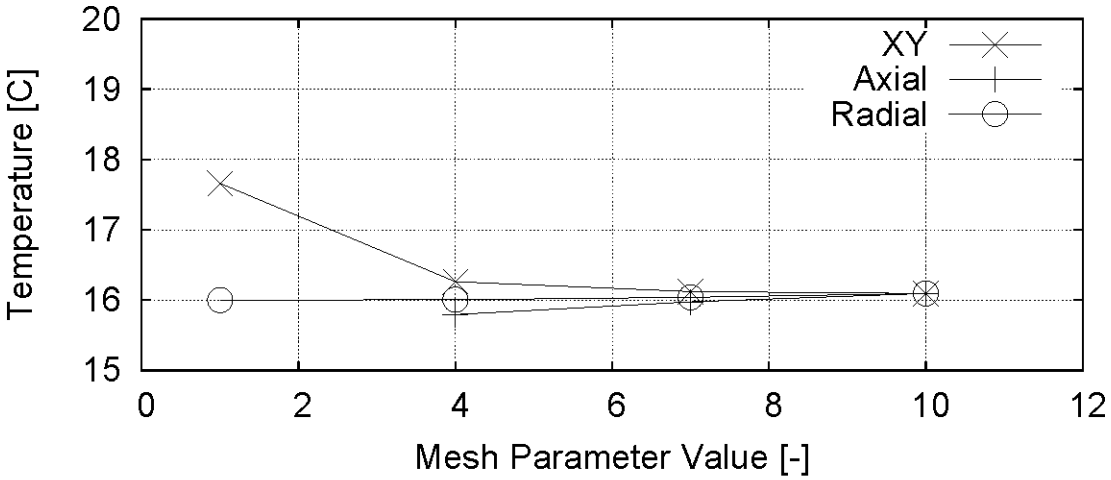

a) Heat exchanger fluid outlet temperature

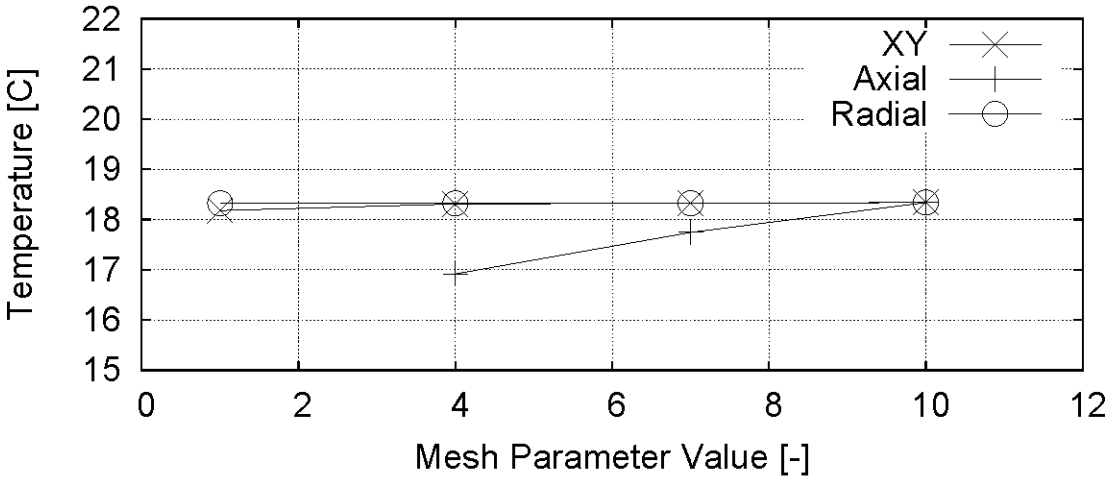

b) Basement wall temperature

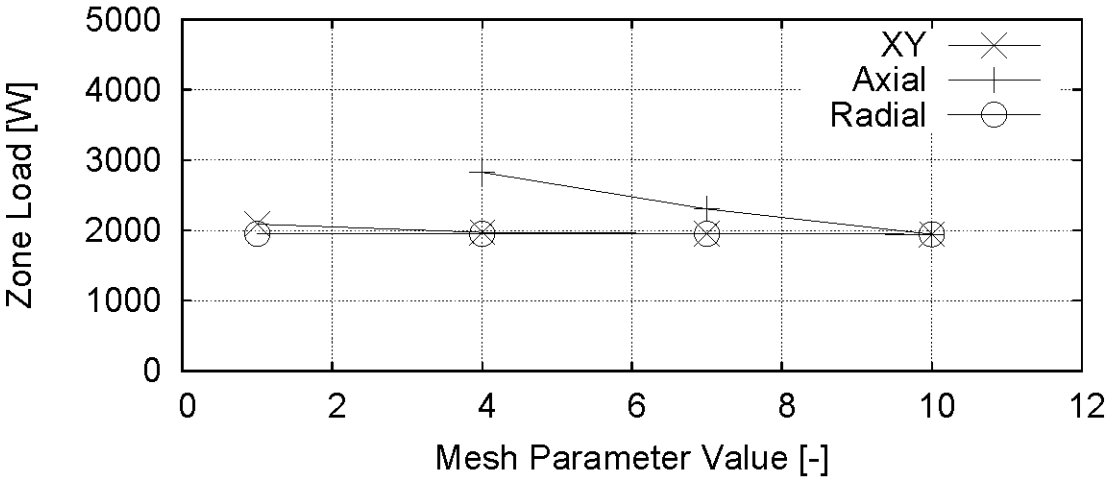

c) Basement zone load

Figure 10: Comparison of analytic and numeric temperatures for validating the accuracy of the coordinate system interface cell

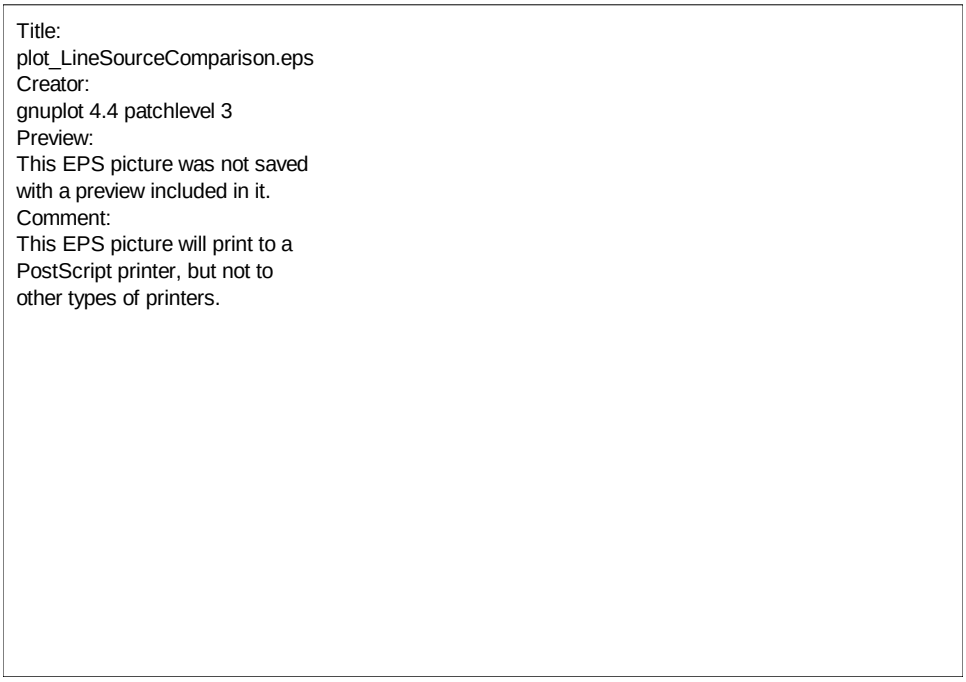

Figure 11: Undisturbed ground temperature results at multiple depths below the ground surface using optimized (parameter estimation) parameters

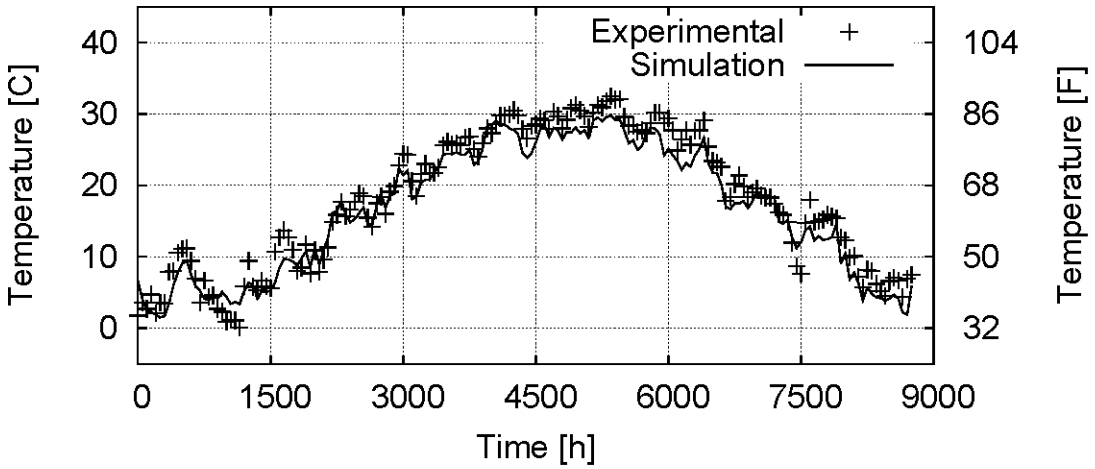

a) Depth = 0.3m (1ft)

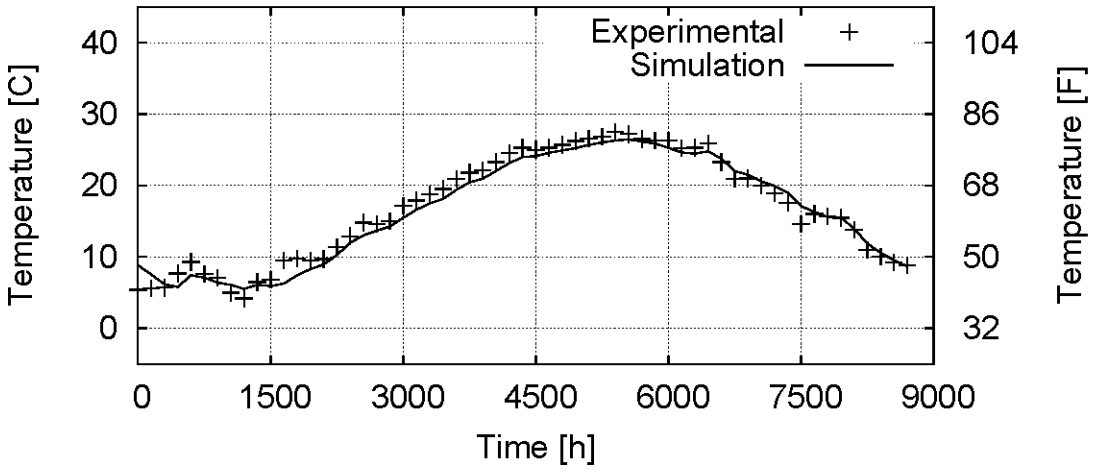

b) Depth = 0.91m (3ft)

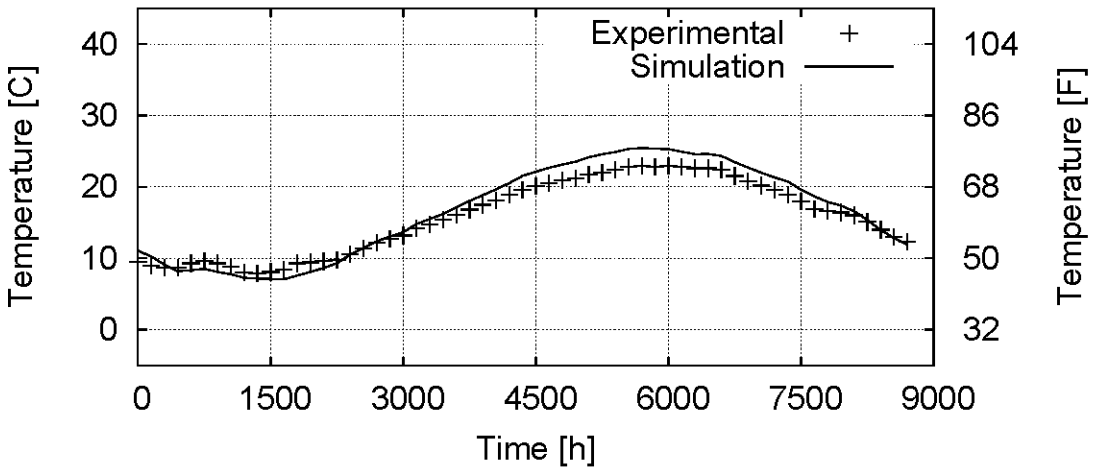

c) Depth = 1.83m (6ft)

Figure 12: Daily averaged heat heat exchanger heat transfer rate validation using experimental measured heat exchanger inlet temperature

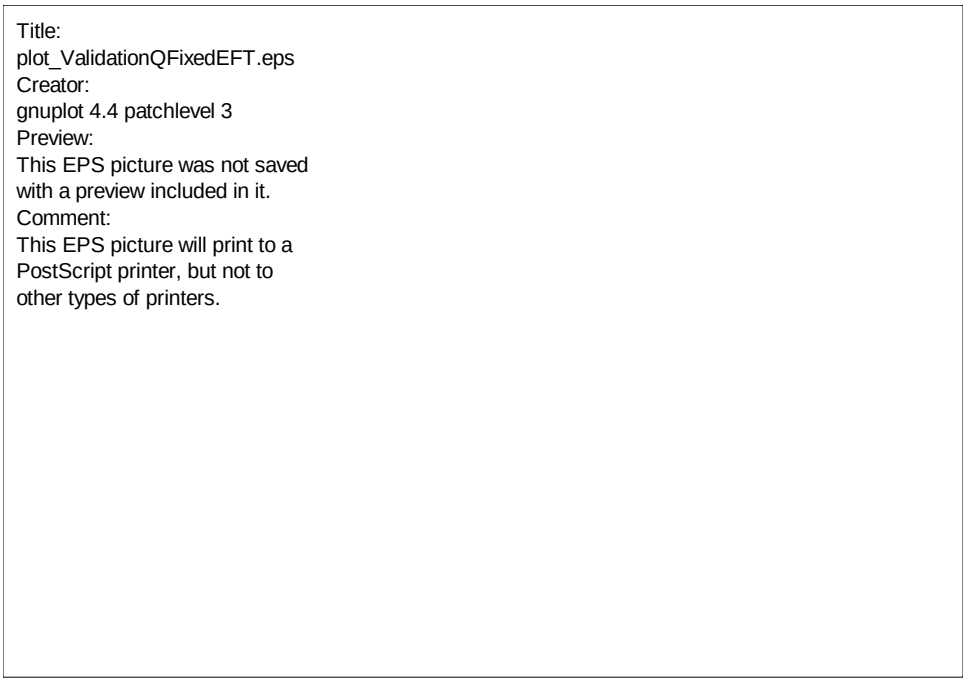

Figure 13: Daily averaged heat pump entering fluid temperature validation using experimental heat transfer to drive a full system simulation

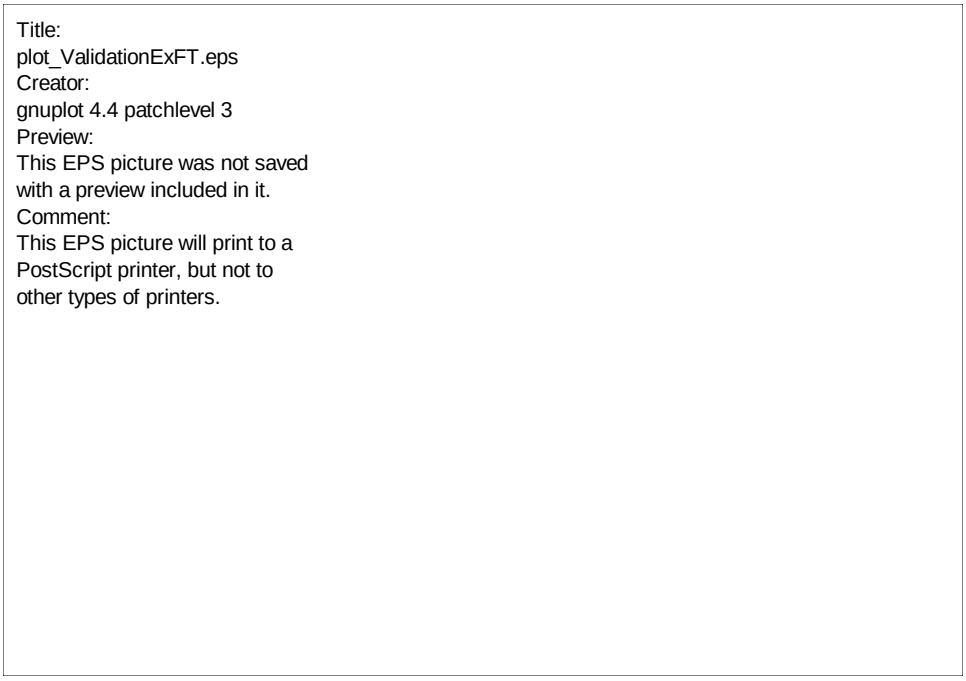

Figure 14: Validation of basement wall heat flux against experimental data